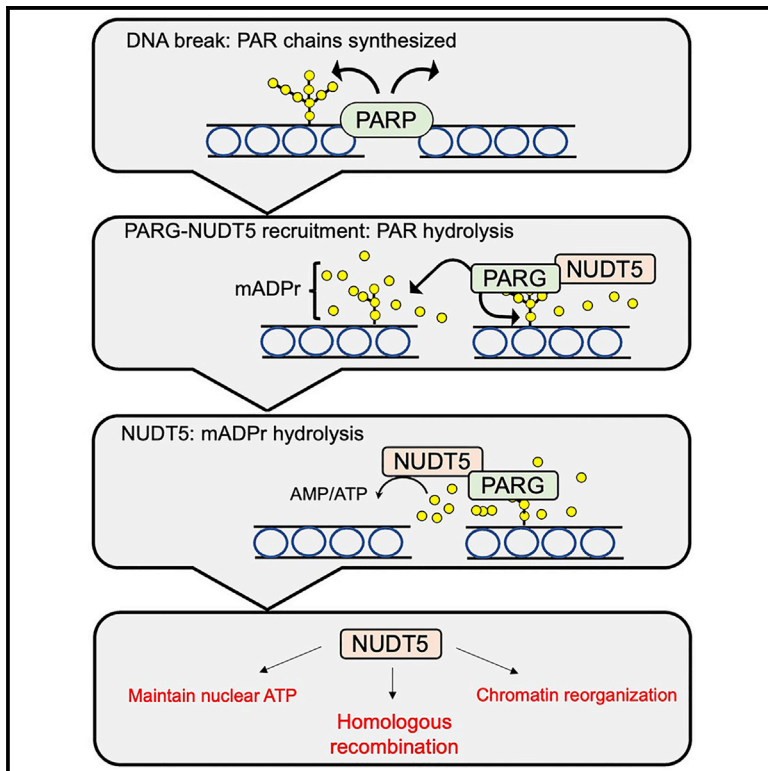# Cell Reports

The ADP-ribose hydrolase NUDT5 is important for DNA repair

Graphical abstract

Authors

Hongyun Qi, Roni Helene Grace Wright, Miguel Beato, Brendan D. Price

Correspondence

brendan_price@dfci.harvard.edu

In brief

Turnover of PAR chains is important for DNA repair. Qi et al. show that NUDT5 is targeted to DNA breaks by PARG, where it hydrolyzes mADP-ribose generated by PARG. NUDT5 functions to maintain nuclear ATP during repair and to support both chromatin remodeling at breaks and homologous recombination.

Highlights

- NUDT5 is a component of the PARP/PARG response to DNA breaks

- PARG is required to position NUDT5 at damage sites

- Mono(ADP-ribose) hydrolysis by NUDT5 contributes to maintenance of nuclear ATP during repair

- Loss of NUDT5 compromises homologous recombination, chromatin remodeling, and repair

CellPress

Report

The ADP-ribose hydrolase NUDT5 is important for DNA repair

Hongyun Qi,[1] Roni Helene Grace Wright,[2] Miguel Beato,[3,4] and Brendan D. Price[1,5,*]

[1]Department of Radiation Oncology, Dana-Farber Cancer Institute, Harvard Medical School, Boston MA 02215, USA
[2]Faculty of Medicine and Health Sciences, Universitat Internacional de Catalunya, Sant Cugat del Vallès, 08195 Barcelona, Spain
[3]Centro de Regulación Genòmica (CRG), The Barcelona Institute of Science and Technology (BIST), 08003 Barcelona, Spain
[4]Universitat Pompeu Fabra (UPF), Barcelona, Spain
[5]Lead contact
*Correspondence: brendan_price@dfci.harvard.edu
https://doi.org/10.1016/j.celrep.2022.111866

SUMMARY

DNA damage leads to rapid synthesis of poly(ADP-ribose) (pADPr), which is important for damage signaling and repair. pADPr chains are removed by poly(ADP-ribose) glycohydrolase (PARG), releasing free mono(ADP-ribose) (mADPr). Here, we show that the NUDIX hydrolase NUDT5, which can hydrolyze mADPr to ribose-5-phosphate and either AMP or ATP, is recruited to damage sites through interaction with PARG. NUDT5 does not regulate PARP or PARG activity. Instead, loss of NUDT5 reduces basal cellular ATP levels and exacerbates the decrease in cellular ATP that occurs during DNA repair. Further, loss of NUDT5 activity impairs RAD51 recruitment, attenuates the phosphorylation of key DNA-repair proteins, and reduces both H2A.Z exchange at damage sites and repair by homologous recombination. The ability of NUDT5 to hydrolyze mADPr, and/or regulate cellular ATP, may therefore be important for efficient DNA repair. Targeting NUDT5 to disrupt PAR/mADPr and energy metabolism may be an effective anti-cancer strategy.

INTRODUCTION

NUDT5 is a member of the nucleoside diphosphates linked to moiety-X (NUDIX) family of hydrolases.[1–5] NUDT5 hydrolyzes mono(ADP-ribose) (mADPr) to ribose-5-phosphate and adenosine-monophosphate (AMP)[1–3,6,7] or, under certain conditions, converts mADPr to ATP. For example, transcriptional activation by the progesterone receptor requires generation of poly(ADP-ribose) (PAR) chains by PAR polymerases (PARPs) to promote chromatin access.[6–10] Hydrolysis of these PAR chains by PAR glycohydrolase (PARG) generates mADPr, which is converted to ATP by NUDT5, generating local ATP to support chromatin remodeling and transcription of hormone-responsive genes.[10] NUDT5 can therefore hydrolyze mADPr to either AMP or ATP.

Replication stress or agents that generate DNA breaks promote recruitment of PARPs to the damage site, where they generate branched PAR chains on the chromatin.[11–13] PAR then recruits repair proteins and chromatin-modifying factors[12,14] that function together to repair the damaged DNA.[15,16] PAR chains are removed by PARG, which cleaves PAR into mADPr units,[11,12] terminating PAR-regulated repair processes. However, mADPr (and pADPr) can function as stress-signaling molecules. For example, PARP activation during ischemia-reperfusion generates free mADPr and pADPr, which bind to apoptosis-inducing factor (AIF)[17,18] and promote cell death through parthanatos.[19] mADPr can also activate the TRPM2 Ca^{2+} channel, promoting cell death during oxidative stress,[20,21] and can promote toxic, non-enzymatic modification

of proteins.[22] Removal of mADPr generated by PARG may therefore be important to regulate potential signaling functions of mADPr during genotoxic stress and DNA repair. Here, we reveal that NUDT5 is a binding partner for PARG and is required for DNA repair by homologous recombination. Further, NUDT5 is required to maintain basal ATP-level functions to maintain ATP levels during ongoing DNA damage/repair. These results indicate that rapid metabolism of mADPr and/or the regulation of cellular ATP by NUDT5 are essential for efficient DNA repair.

RESULTS

NUDT5 and homologous recombination

The major repair pathways for DNA double-strand breaks (DSBs) include homologous recombination (HR), direct ligation of DNA ends by classical non-homologous end joining (cNHEJ) and repair by microhomology-mediated end joining (alternative EJ [alt-EJ]). We used reporters of these pathways to determine if NUDT5 contributes to DSB repair. Small interfering RNAs (siRNAs) targeting NUDT5 (Figure S1A) decreased repair by HR (Figure 1A) but did not alter repair by cNHEJ (Figure 1A) or alt-EJ (Figure S1B). The NUDT5 inhibitor TH5427[6] also suppressed HR without altering cNHEJ (Figure 1B) or alt-EJ (Figure S1B), indicating that NUDT5's catalytic activity is important for HR. Further, TH5427 elicited a small, but significant, increase in sensitivity to radiation (Figure 1C), consistent with a role for NUDT5 in DSB repair. siRNA to NUDT5 did not alter cell-cycle
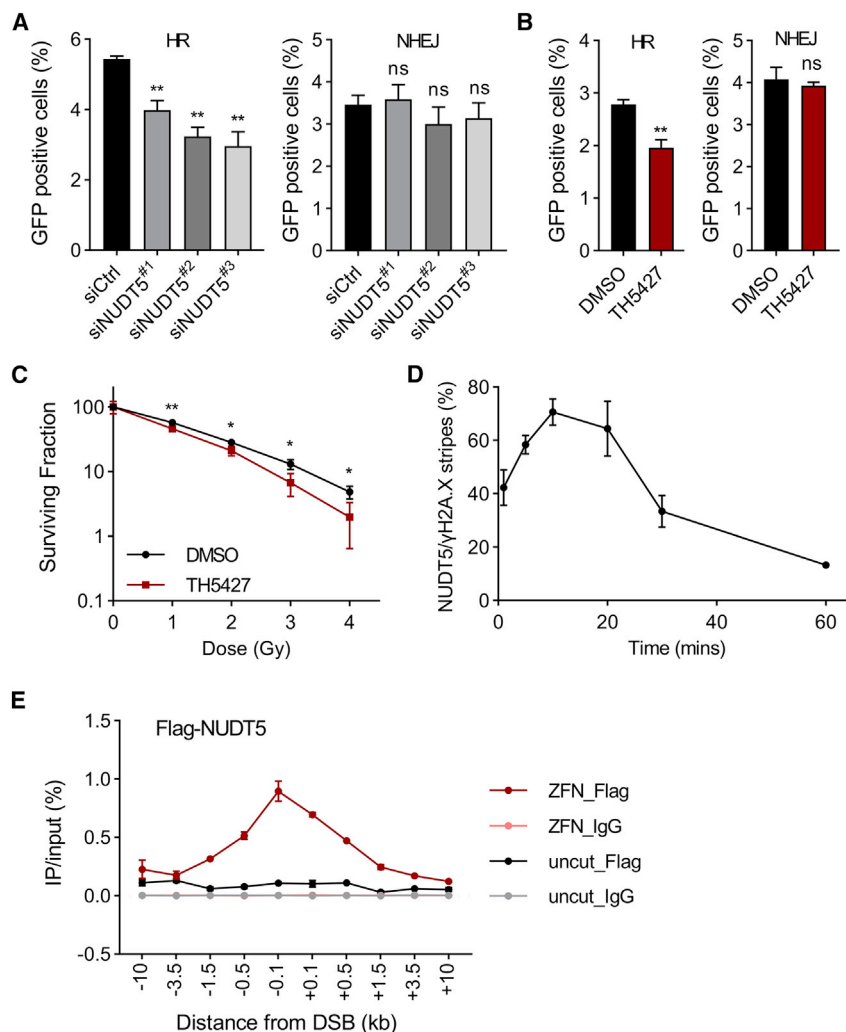
Figure 1. NUDT5 depletion impairs repair by HR

(A) U2OS DR-GFP (HR) or HeLa EJ5-GFP (NHEJ) cell reporters were transfected with control or NUDT5 siRNAs followed by I-SceI and analyzed for GFP by fluorescence-activated cell sorting (FACS) 48 h later. Data are mean ± SEM (n = 3).

(B) DR-GFP or EJ5-GFP cells were treated with TH5427 (10 μM) for 4 h followed by I-SceI and analyzed for GFP after 48 h. Data are mean ± SEM (n = 3 biological replicates).

(C) U2OS cells were preincubated with TH5427 (10 μM) for 4 h and irradiated, and surviving colonies were counted after 12 days. Data are mean ± SEM (n = 3 biological replicates).

(D) Following laser striping, cells were allowed to recover for 10 min, followed by immunofluorescent staining for γH2AX and NUDT5. The percentage of γH2A.X-positive DNA-damage tracks with NUDT5 were scored (see Figure S2B for representative images). Data are mean ± SEM (n = 3 biological replicates), 50 cells per replicate.

(E) 293T cells expressing FLAG-NUDT5 were transfected with p84-ZFN and processed for ChIP using FLAG antibody or IgG control. ChIP signals are IP DNA/input DNA (%). Data are mean ± SEM (n = 2 biological replicates).

All data analyzed using unpaired two-tailed Student's test. *p < 0.05, **p < 0.01.

kinetics (Figure S1C), indicating that NUDT5 does not alter HR by altering cell-cycle progression. Further, RNA sequencing (RNA-seq) analysis indicated that siRNA to NUDT5 did not alter expression of other NUDIX family members (Figures S1D and S1F) or HR proteins (Figure S1E).

To monitor NUDT5 recruitment to DNA breaks, DNA damage was generated using a laser, followed by immunofluorescent staining for NUDT5 and γH2AX. NUDT5 accumulated on damaged chromatin, with maximal recruitment 10–20 min post-damage (Figures 1D and S2B). In addition, we generated a DSB using the p84 zinc finger nuclease (p84-ZFN)[23] coupled with chromatin immunoprecipitation (ChIP) to monitor FLAG-NUDT5. Minimal ChIP signal for NUDT5 was detected with immunoglobulin G (IgG) or in the absence of a DSB, whereas DSB production led to increased FLAG-NUDT5 at the DSB (Figure 1E). NUDT5 is therefore rapidly localized to DNA breaks.

NUDT5 is linked with PAR metabolism,[1,7,10] and PARylation recruits repair proteins to damage sites.[11] We therefore determined if NUDT5 recruitment to DSBs required PARP, which

PARylates the chromatin, or PARG, which hydrolyzes pADPr chains. When PARG was targeted with siRNA (Figure S2A), NUDT5 recruitment was blocked (Figures 2A and S2B), even though PAR levels were elevated (Figures 2B and S2C). PARG recruitment to damaged chromatin requires interaction with PAR. The PARP inhibitor olaparib blocked PARylation and recruitment of both PARG and NUDT5 (Figures 2C and S2D). Further, PARG and NUDT5 interact[10] (Figure S2E). NUDT5 recruitment to damage sites therefore requires PARG but not PAR. Finally, loss of NUDT5 did not alter the recruitment of PARG (Figure S2F) or the kinetics or intensity of PARylation/dePARylation during repair (Figures S2G and S2H). We conclude that PARG recruits NUDT5 to sites of damage but that NUDT5 does not regulate PARG catalytic activity or PAR turnover.

NUDT5 and nuclear ATP

Because NUDT5 can hydrolyze mADPr to ATP,[6,10] we examined if NUDT5 contributed to ATP levels during DNA damage. Among damaging agents, H_2O_2 (100 μM) generated the highest levels of PAR (Figures S2I and S2J), indicating that hydrolysis of this PAR would yield the highest levels of mADPr. Exposure to H_2O_2 led to a slow decline in cellular ATP over time (Figure 2D). NUDT5 inhibition with TH5427 (Figure 2D) or siNUDT5 (Figure 2E) led to a larger reduction in total ATP during H_2O_2 exposure. Because PAR, PARG, and NUDT5 operate in the nucleus, we also used a GFP-luciferase ATP reporter with a nuclear
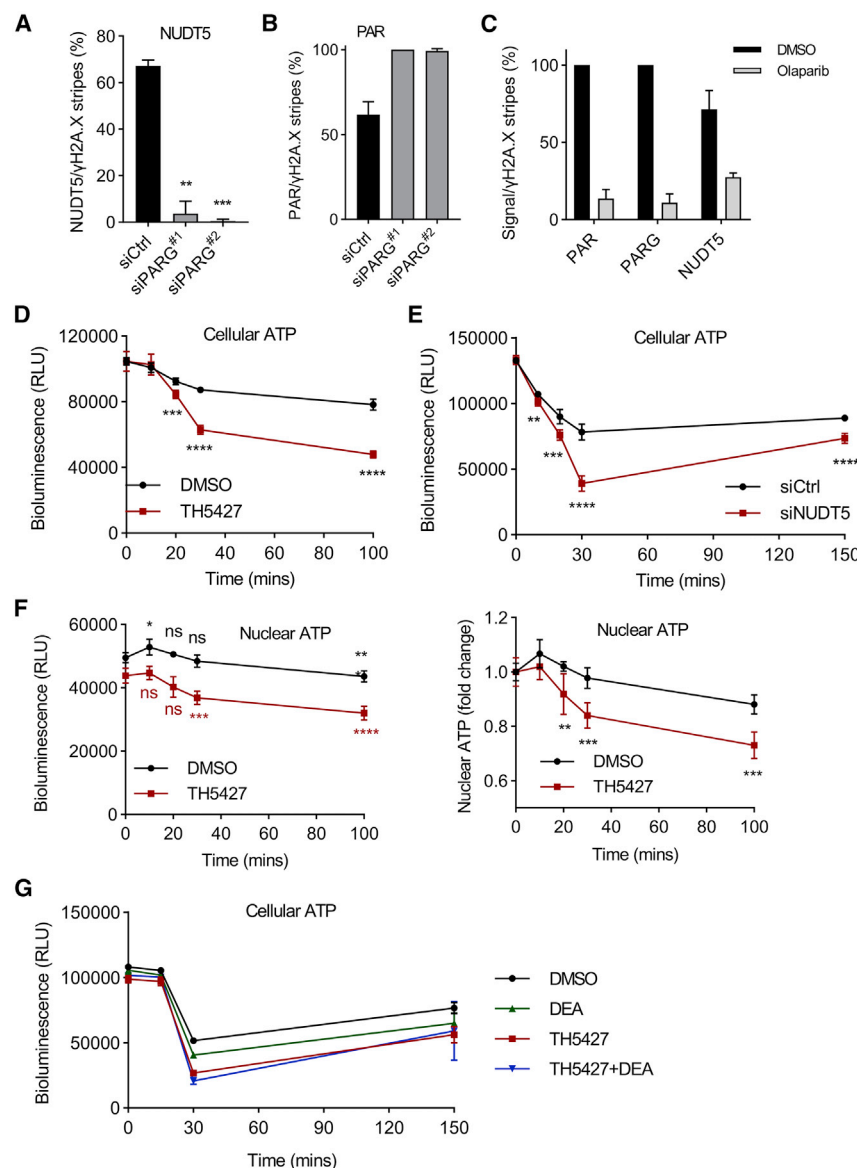
Figure 2. NUDT5 recruitment to sites of DNA damage requires PARG

(A and B) U2OS cells were transfected with control or PARG siRNAs, exposed to laser striping, and allowed to recover for 10 min, followed by immunofluorescent staining for γH2AX and NUDT5 (A) or γH2AX and PAR (B). The percentage of γH2AX-positive DNA-damage tracks with NUDT5 (A) or PAR (B) was scored. Data are mean ± SEM (n = 2 biological replicates for A, n = 3 for B), 50 cells per replicate.

(C) U2OS cells were treated with olaparib (5 μM) for 1 h before laser striping. Following recovery for 1 (PAR) or 10 min (PARG and NUDT5), cells were stained for γH2AX and either PAR, PARG, or NUDT5. Data are mean ± SEM (n = 2 biological replicates), 50 cells per replicate.

(D) U2OS cells were preincubated in DMSO or TH5427 (10 μM) for 4 h, followed by H_2O_2 (100 μM) and cellular ATP measured using ATP-Glo. Data are mean ± SEM (n = 6).

(E) U2OS cells were transfected with control or NUDT5 siRNA, followed by H_2O_2 (100 μM) and cellular ATP measured using ATP-Glo. Data are mean ± SEM (n = 6 biological replicates).

(F) U2OS cells expressing GFP-NucLuc ATP reporter were treated with TH5427 (10 μM) for 4 h, followed by H_2O_2 (100 μM) and nuclear ATP measured. Total signal (left) and fold change relative to untreated (right) shown. Data are mean ± SEM (n = 6 biological replicates).

(G) U2OS cells were preincubated in DMSO, TH5427 (10 μM, 4 h), or DEA (1 μM, 1 h), or in combination, followed by H_2O_2 (100 μM) and cellular ATP measured using ATP-Glo. Data are mean ± SEM (n = 4 biological replicates).

All data analyzed using unpaired two-tailed Student's test. *p < 0.05, **p < 0.01.

localization signal (GFP-NucLuc).[10,24] GFP-NucLuc is localized to the nucleus (Figure S2K), and inhibition of ATP synthesis by mitochondria or glycolysis reduced the signal from the reporter (Figure S2L). Using this nuclear ATP reporter, TH5427 reduced basal ATP levels in the nucleus (Figure 2F) of multiple cell lines (Figure S3A). This reduced basal nuclear ATP implies a role for NUDT5 in regulating basal ATP levels. H_2O_2 exposure led to a small, but significant, decrease in nuclear ATP (Figure 2F), broadly reflecting changes in ATP seen at the whole-cell level (Figures 2D and 2E). Finally, NUDT5 inhibition resulted in a larger decline in nuclear ATP after DNA damage (Figure 2F). Loss of NUDT5 is therefore associated with reduced nuclear ATP during DNA repair. Prolonged (hours) PARP activation leads to ATP depletion due to the use of ATP to re-synthesize NAD+, which may contribute to the observed decline in ATP during DNA damage/repair. However, PARP inhibition did not

alter the reduction in ATP during repair (Figure S3B), indicating that PARylation by PARPs does not contribute to the observed changes in ATP.

Next, we inhibited PARG, which hydrolyzes PAR to mADPr, the substrate for NUDT5. PARG inhibition with DEA led to a more pronounced drop in cellular ATP after damage (Figure 2G). Combining PARG inhibition with NUDT5 inhibition was not additive (Figure 2G), indicating that PARG and NUDT5 may operate in the same pathway. mADPr contributed by PARG hydrolysis of PAR may therefore be important for NUDT5's ability to regulate ATP during DNA damage. Finally, because loss of NUDT5 correlates with reduced nuclear ATP (Figures 2D and 2F) but only affects DSB repair by HR (Figure 1A), we tested if ATP reduction specifically inhibits HR. 2-deoxyglucose (2-DG), which blocks glycolysis and reduces ATP (Figures S2L and S3C), reduced repair by HR, while cNHEJ and alt-EJ were unaffected (Figure S3D). 2-DG had minimal impact on cell-cycle position (Figure S3E). HR is therefore more dependent on nuclear ATP than either cNHEJ or alt-EJ.
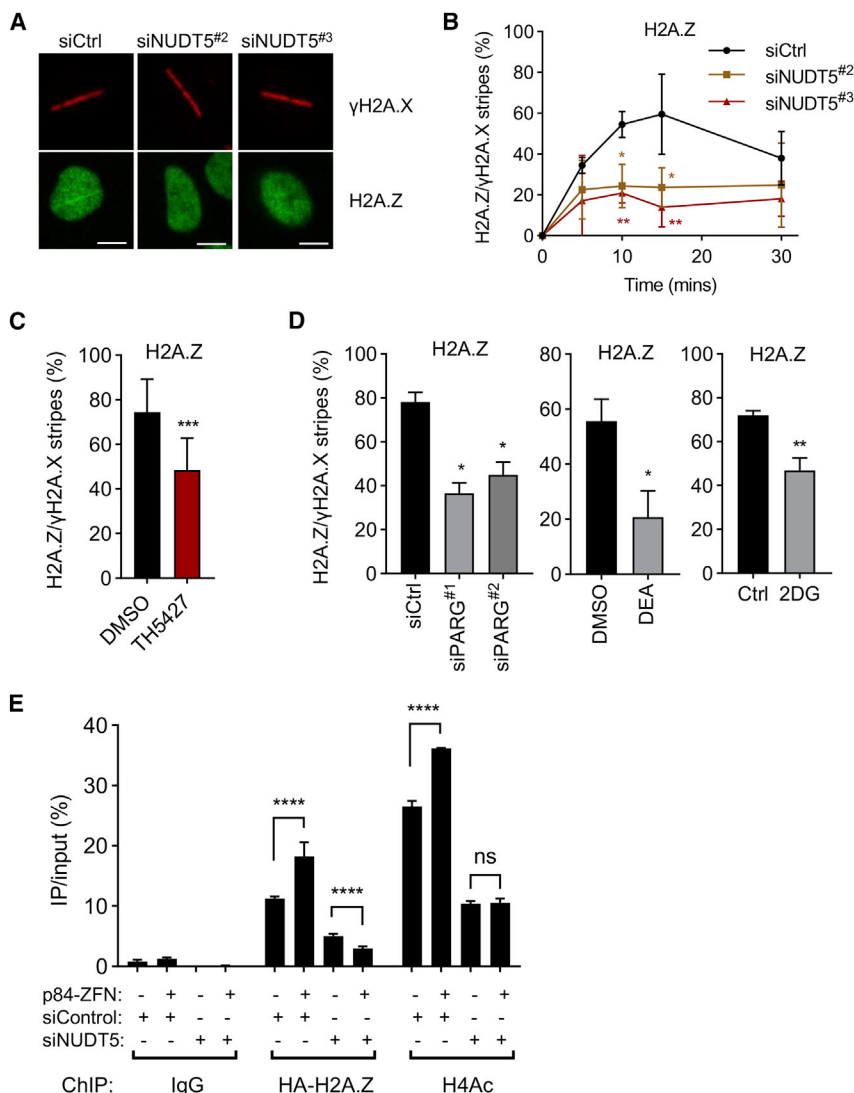
Figure 3. NUDT5 regulates H2A.Z exchange during repair

(A and B) U2OS cells were transfected with control or NUDT5 siRNAs and exposed to laser striping, followed by immunofluorescent staining for γH2AX and H2A.Z. γH2A.X-positive DNA-damage tracks with H2A.Z were scored. Data are mean ± SEM (n = 3 biological replicates), 50 cells per replicate. Scale bar, 10 μm.

(C) U2OS cells were pretreated with TH5427 (10 μM) for 4 h, exposed to laser microirradiation, and the percentage of γH2AX-positive stripes with H2A.Z were measured 10 mins later. Data are mean ± SEM (n = 3 biological replicates), 50 cells per replicate.

(D) U2OS cells were transfected with control or PARG siRNA (left) or preincubated with DEA (1 μM/1 h) or 2-DG. Following laser microirradiation (10 min), the percentage of γH2AX-positive stripes with H2A.Z was scored. Data are mean ± SEM (n = 2 biological replicates), 50 cells per replicate.

(E) 293T cells expressing HA-H2A.Z were transfected with control or NUDT5 siRNA, followed by p84-ZFN and ChIP using IgG, hemagglutinin (HA) antibody, or H4Ac antibody. qPCR used primers located 1.5 kb from the DSB. Results are IP/input DNA (%). Data are mean ± SEM (n = 2 biological replicates).

All data analyzed using unpaired two-tailed Student's test. *p < 0.05, **p < 0.01, and ***p < 0.001.

NUDT5 and H2A.Z exchange

ATP production by NUDT5 promotes chromatin reorganization by ATP-driven remodeling complexes.[10] DSB repair utilizes the NuA4-TIP60 remodeling complex,[23,25–28] which exchanges histone H2A.Z at DSBs and increases acetylation of histone H4 (H4Ac).[23,27] H2A.Z accumulated on damaged chromatin (Figures 3A and 3B) and siRNA to NUDT5 (Figure 3B) or the NUDT5 inhibitor TH5427 (Figure 3C) both attenuated H2A.Z exchange. siRNA to PARG (which blocks recruitment of NUDT5; Figure 2A) also inhibited H2A.Z exchange (Figure 3D). Next, we used the PARG inhibitor DEA to block mADPr production and starve NUDT5 of its substrate. DEA reduced H2A.Z exchange (Figure 3D) but did not block NUDT5 recruitment to the site of damage (Figure S4A). The catalytic activity of both PARG and NUDT5 are therefore required for H2A.Z exchange at DSBs. In addition, ATP depletion with 2DG reduced H2A.Z exchange (Figure 3D) but did not alter PARG recruitment, PAR production, or NUDT5 recruitment (Figure S4B), consistent

with H2A.Z exchange being ATP dependent. Finally, H2A.Z exchange is required for acetylation of histone H4 at DSBs.[25] We used the p84-ZFN to create a DSB, followed by ChIP for HA-H2A.Z and H4Ac. Interestingly, NUDT5 siRNA reduced basal H2A.Z and H4Ac at the p84-ZFN site in the absence of a DSB (Figure 3E), which may reflect the reduction in nuclear ATP observed in the absence of NUDT5 (Figure 2F) and/or a broader role for NUDT5 in regulating H4Ac and H2A.Z. However, when DSBs were generated, both H2A.Z exchange and H4Ac at DSBs were reduced in the absence of NUDT5 (Figure 3E), consistent with the requirement for NUDT5 to promote H2A.Z exchange.

NUDT5 and signaling during repair

siRNA to NUDT5 delayed the appearance and resolution of γH2AX foci (Figure 4A), consistent with a repair defect. Loss of NUDT5 also led to a small reduction in phosphorylation of H2AX and KAP1 after DNA damage (Figures S4C–S4E), perhaps reflecting reduced overall ATP in the cells. NUDT5 is important for HR but not NHEJ (Figures 1A and 1B). siRNA to NUDT5 reduced the recruitment of the HR-specific RAD51 but not 53BP1 (Figure 4B). Loss of NUDT5 also led to a reduction in RPA foci (Figure 4C), implying reduced end resection at DNA breaks. Further, there was a small, but significant, increase in the accumulation of the REV7 subunit of the SHIELDIN complex at DNA breaks (Figure 4D). SHIELDIN limits end resection and
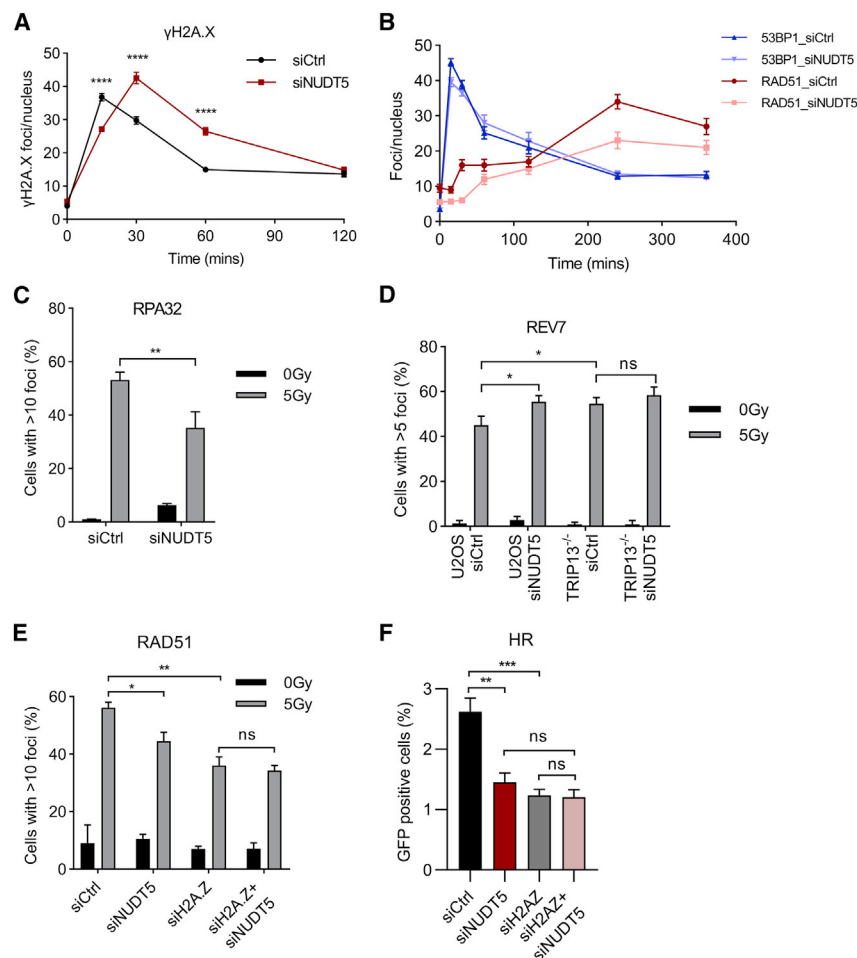
Figure 4. NUDT5 regulates HR signaling events

(A) U2OS cells were transfected with control or NUDT5 siRNA for 48 h and irradiated (1 Gy), followed by immunofluorescent staining for γH2AX. Average foci number per cell was calculated. Data are mean ± SEM (n = 3 biological replicates), 50 cells per replicate.

(B) U2OS cells were transfected with control or NUDT5 siRNA for 48 h and irradiated (5 Gy), and immunofluorescent staining for 53BP1 or RAD51 was carried out. Average foci number per cell was calculated. Data are mean ± SEM (n = 3 biological replicates), 50 cells per replicate.

(C) U2OS cells were transfected with control or NUDT5 siRNA for 48 h and irradiated (5 Gy), and immunofluorescent staining for RPA32 was carried out 6 h later. The percentage of cells with >10 foci was calculated. Data are mean ± SEM (n = 3 biological replicates) with 50 cells per replicate.

(D) U2OS cells or TRIP13 knockout U2OS cells were transfected with control or NUDT5 siRNA for 48 h, irradiated (5 Gy), and allowed to recover for 6 h, followed by immunofluorescent staining for REV7. The percentage of cells with >5 foci was calculated. Data are mean ± SEM (n = 3 biological replicates), 50 cells per replicate.

(E) DR-GFP (HR) reporter cells were transfected with control siRNA or siRNA to NUDT5 or H2A.Z and irradiated (5 Gy), and immunofluorescent staining for RAD51 was carried out 4 h later. Percentage of cells with >10 foci was calculated. Data are mean ± SEM (n = 3 biological replicates), 100 cells per replicate.

(F) DR-GFP (HR) reporter cells were transfected with either control siRNA, NUDT5 siRNA, H2A.Z siRNA, or both. Cells were transfected with I-Sce1 24 h later to initiate HR, then analyzed by FACS for GFP expression 48 h later. Data are mean ± SEM (n = 3 biological replicates).

All data analyzed using unpaired two-tailed Student's test. *p < 0.05, **p < 0.01, ***p < 0.001, and ****p < 0.0001.

favors repair by end joining over HR.[29–32] The accumulation of REV7 in the absence of NUDT5 was similar to that seen in the absence of TRIP13, which removes REV7 from the chromatin.[33] Further, siRNA to either H2A.Z or NUDT5 (Figure S4F) reduced RAD51 foci (Figure 4E) and HR (Figure 4F) to similar extents. However, co-depletion of H2A.Z and NUDT5 did not further reduce either RAD51 (Figure 4E) or HR (Figure 4F), implying that NUDT5 and H2A.Z function in the same pathway to promote DSB repair by HR.

DISCUSSION

NUDT5 is important for repair by HR but did not contribute to repair by cNHEJ or alt-EJ. Loss of NUDT5 led to defects in HR, including reductions in H2A.Z exchange, H4 acetylation, and RAD51 recruitment, but increased levels of the SHIELDIN component REV7.[29,30,33,34] REV7 limits end resection and favors repair by cNHEJ, consistent with the reduction in RAD51 and HR observed in the absence of NUDT5. Further, loss of either H2A.Z or NUDT5 reduced HR to the same extent, but loss of both was not additive, indicating that NUDT5

and H2A.Z are in the same pathway. NUDT5 may function, at least in part, to support the NuA4/H2A.Z/HR pathway during repair.

HR was dependent on NUDT5's catalytic activity, indicating that the ability of NUDT5 to hydrolyze mADPr is important for repair. NUDT5 is recruited to sites of DNA damage by PARG, positioning NUDT5 directly at DNA breaks. PARG cleaves mADPr units from PAR chains,[13,35,36] and PARG inhibition has similar phenotypic effects to PARP inhibition on DNA repair,[37] indicating that PAR disassembly is key to efficient repair. The close spatial positioning of PARG and NUDT5 at DNA breaks may allow mADPr generated by PARG to be directly hydrolyzed by NUDT5, limiting local mADPr accumulation, which might have negative impacts on repair. NUDT5 is therefore part of the PARP/PARG-directed response to DNA damage in which PARylation/dePARylation regulates recruitment of repair proteins and chromatin structure at damage sites.[11]

NUDT5 hydrolyzes free mADPr to ribose-5-phosphate and AMP.[1,7,10,38,39] However, during PAR-dependent activation of the progesterone transcriptional program, PAR hydrolysis by PARG generates mADPr, which is then converted to ATP, rather

than AMP, by NUDT5.[6,7,10,40] This provides the energy to maintain nuclear ATP levels and support transcription.[10] Here, loss of NUDT5 reduced basal nuclear ATP levels and evoked a larger reduction in nuclear ATP during DNA repair, consistent with a role for NUDT5 in supporting nuclear ATP levels during DNA repair. The reduction in ATP levels during repair was mimicked by inhibiting PARG, which blocks production of NUDT5's substrate mADPr. NUDT5's catalytic activity and a supply of mADPr from PARG are therefore important for NUDT5 to regulate ATP levels. A simple interpretation would be that NUDT5 converts a fraction of the mADPr to ATP, providing locally elevated levels of ATP to support repair. In support of this, loss of NUDT5 was associated with reduced activity of multiple ATP-dependent repair pathways, including phosphorylation of H2AX and KAP1, reduced activity of the NuA4 remodeling ATPase,[23,25,26,28,41,42] and reduced removal of REV7 by the TRIP13 AAA+ ATPase.[33,34] In the absence of NUDT5, reduced local ATP at repair sites may limit multiple ATP-dependent steps, resulting in reduced RAD51 loading and limiting HR-mediated repair. However, technical limitations prevent us from directly demonstrating that NUDT5 synthesizes ATP from mADPr at sites of DNA damage. The observation that cNHEJ and alt-EJ were both insensitive to loss of NUDT5, despite sharing many ATP-driven pathways with HR, indicates that either cNHEJ is only weakly dependent on ATP or that there is a rate-limiting step in HR that requires ATP generation by NUDT5. Further, ATP levels are dynamically regulated at many levels, including altered mitochondrial activity, increased metabolic flux through the tricarboxylic acid (TCA) cycle, or changes in energy-utilizing pathways regulated by, e.g., AMP kinase. NUDT5 may potentially alter ATP metabolism indirectly through regulation of these pathways. It is also possible that NUDT5's ability to remove mADPr (rather than generate ATP/AMP) may contribute to its regulation of HR and repair. mADPr is a stress signaling molecule.[43] For example, elevated mADPr can bind to the TRPM2 Ca^{2+} channel, regulating Ca^{2+} gradients during oxidative stress,[44] or promote toxic ADP-ribosylation of proteins.[22] Further, chronic PARP activation (e.g., genotoxic stress or inflammatory injury) leads to toxic accumulation of pADPr/mADPr, which can bind to and activate AIF-associated nucleases that mediate cell death via parthanatos.[18] mADPr removal by NUDT5 during repair may therefore limit toxicity associated with elevated levels of mADPr. PAR and mADPr can also bind to macrodomains and related structures, which may interfere with the activity of macrodomain-containing DNA-repair proteins, leading to the observed reduction in HR. Thus, NUDT5 may regulate HR-mediated repair through multiple pathways (Figure S5), including (1) regulating the levels of the stress signaling molecule mADPr; (2) generating ATP at damage sites to support local repair; and/or (3) by modulating cellular ATP pools independently of damage. The relative contribution of these three activities of NUDT5 to HR remains to be determined.

NUDT5 is overexpressed in most cancers[6,7,10,45,46] and is associated with reduced patient survival.[7,10,46] Tumor cells prioritize glycolysis for ATP production (Warburg effect[47]) despite the ability of OXPHOS to generate higher levels of ATP. This may allow tumors to survive better in fluctuating oxygen conditions, to generate NADPH for anti-oxidant defenses, and to use

glycolysis intermediates to synthesize metabolites required for proliferation. As such, there is an ongoing effort to target glycolysis as an anti-tumor strategy. Tumors also experience ongoing genomic instability, making them dependent on effective DNA-repair pathways for survival. NUDT5 may allow tumor cells experiencing genomic instability (and elevated PARylation/dePARylation) to rapidly hydrolyze mADPr generated by PARG, limiting toxic accumulation of mADPr, as well as providing a pathway to maintain adequate nuclear ATP levels during genotoxic stress. Consequently, inhibition of NUDT5, either alone or in combination with cancer therapies, may be an effective strategy for targeting energy metabolism in tumor cells. Finally, NUDT5 is a component of the cellular PARylation/dePARylation machinery that regulates mADPr and ATP pools, which are important for DNA repair.

Limitations of the study

Currently, the exact mechanistic details about how NUDT5 regulates HR are unclear. Although our data indicate that NUDT5's catalytic activity is essential for HR, distinguishing whether this is due to removal of mADPr or production of AMP/ATP at damage sites by NUDT5 is not known. The ability to monitor ATP (and mADPr) levels directly at damage sites would provide a key tool to address this issue. Further, it remains possible that despite NUDT5 being recruited to DSBs and being required for H2A.Z exchange at DSBs, NUDT5 may interact with other nuclear systems that regulate ATP or mADPr independently of its presence at damage sites. In this scenario, NUDT5 may indirectly influence HR by altering overall nuclear ATP or mADPr levels. Establishing the protein interaction network of NUDT5 and techniques to monitor ATP levels, coupled with an understanding of how NUDT5's complex catalytic activities contribute to HR, will be fruitful areas for future studies.

STAR★METHODS

Detailed methods are provided in the online version of this paper and include the following:

- KEY RESOURCES TABLE
- RESOURCE AVAILABILITY
  - Lead contact
  - Materials availability
  - Data and code availability
- EXPERIMENTAL MODEL AND SUBJECT DETAILS
  - Cell lines and reagents
- METHODS DETAILS
  - Cell lines and transfection
  - DSB repair reporter assays
  - Clonogenic cell survival assay
  - ATP measurement
  - Laser microirradiation
  - DSB generation and ChIP assays
  - Co-immunoprecipitation
  - RNA-seq
  - Irradiation-induced foci assay
  - Cell cycle analysis
- QUANTIFICATION AND STATISTICAL ANALYSIS

REFERENCES

1. Palazzo, L., Thomas, B., Jemth, A.S., Colby, T., Leidecker, O., Feijs, K.L.H., Zaja, R., Loseva, O., Puigvert, J.C., Matic, I., et al. (2015). Processing of protein ADP-ribosylation by Nudix hydrolases. Biochem. J. 468, 293–301. https://doi.org/10.1042/BJ20141554.

2. Daniels, C.M., Thirawatananond, P., Ong, S.E., Gabelli, S.B., and Leung, A.K.L. (2015). Nudix hydrolases degrade protein-conjugated ADP-ribose. Sci. Rep. 5, 18271. https://doi.org/10.1038/srep18271.

3. Zha, M., Guo, Q., Zhang, Y., Yu, B., Ou, Y., Zhong, C., and Ding, J. (2008). Molecular mechanism of ADP-ribose hydrolysis by human NUDT5 from structural and kinetic studies. J. Mol. Biol. 379, 568–578. https://doi.org/10.1016/j.jmb.2008.04.006.

4. McLennan, A.G. (2006). The Nudix hydrolase superfamily. Cell. Mol. Life Sci. 63, 123–143. https://doi.org/10.1007/s00018-005-5386-7.

5. Hashiguchi, K., Hayashi, M., Sekiguchi, M., and Umezu, K. (2018). The roles of human MTH1, MTH2 and MTH3 proteins in maintaining genome stability under oxidative stress. Mutat. Res. 808, 10–19. https://doi.org/10.1016/j.mrfmmm.2018.01.002.

6. Page, B.D.G., Valerie, N.C.K., Wright, R.H.G., Wallner, O., Isaksson, R., Carter, M., Rudd, S.G., Loseva, O., Jemth, A.S., Almlöf, I., et al. (2018). Targeted NUDT5 inhibitors block hormone signaling in breast cancer cells. Nat. Commun. 9, 250. https://doi.org/10.1038/s41467-017-02293-7.

7. Carreras-Puigvert, J., Zitnik, M., Jemth, A.S., Carter, M., Unterlass, J.E., Hallström, B., Loseva, O., Karem, Z., Calderón-Montaño, J.M., Lindskog, C., et al. (2017). A comprehensive structural, biochemical and biological profiling of the human NUDIX hydrolase family. Nat. Commun. 8, 1541. https://doi.org/10.1038/s41467-017-01642-w.

8. Wright, R.H.G., Castellano, G., Bonet, J., Le Dily, F., Font-Mateu, J., Ballaré, C., Nacht, A.S., Soronellas, D., Oliva, B., and Beato, M. (2012). CDK2-dependent activation of PARP-1 is required for hormonal gene regulation in breast cancer cells. Genes Dev. 26, 1972–1983. https://doi.org/10.1101/gad.193193.112.

9. Wright, R.H.G., and Beato, M. (2012). PARty promoters: hormone-dependent gene regulation requires CDK2 activation of PARP1. Cell Cycle 11, 4291–4293. https://doi.org/10.4161/cc.22531.

10. Wright, R.H.G., Lioutas, A., Le Dily, F., Soronellas, D., Pohl, A., Bonet, J., Nacht, A.S., Samino, S., Font-Mateu, J., Vicent, G.P., et al. (2016). ADP-ribose-derived nuclear ATP synthesis by NUDIX5 is required for chromatin remodeling. Science 352, 1221–1225. https://doi.org/10.1126/science.aad9335.

11. Qi, H., Price, B.D., and Day, T.A. (2019). Multiple roles for mono- and poly(ADP-ribose) in regulating stress responses. Trends Genet. 35, 159–172. https://doi.org/10.1016/j.tig.2018.12.002.

12. Gupte, R., Liu, Z., and Kraus, W.L. (2017). PARPs and ADP-ribosylation: recent advances linking molecular functions to biological outcomes. Genes Dev. 31, 101–126. https://doi.org/10.1101/gad.291518.116.

13. Barkauskaite, E., Jankevicius, G., and Ahel, I. (2015). Structures and mechanisms of enzymes employed in the synthesis and degradation of PARP-dependent protein ADP-ribosylation. Mol. Cell 58, 935–946. https://doi.org/10.1016/j.molcel.2015.05.007.

14. Luijsterburg, M.S., de Krijger, I., Wiegant, W.W., Shah, R.G., Smeenk, G., de Groot, A.J.L., Pines, A., Vertegaal, A.C.O., Jacobs, J.J.L., Shah, G.M., and van Attikum, H. (2016). PARP1 links CHD2-mediated chromatin expansion and H3.3 deposition to DNA repair by non-homologous end-joining. Mol. Cell 61, 547–562. https://doi.org/10.1016/j.molcel.2016.01.019.

15. Eustermann, S., Wu, W.F., Langelier, M.F., Yang, J.C., Easton, L.E., Riccio, A.A., Pascal, J.M., and Neuhaus, D. (2015). Structural basis of detection and signaling of DNA single-strand breaks by human PARP-1. Mol. Cell 60, 742–754. https://doi.org/10.1016/j.molcel.2015.10.032.

16. Thomas, C.J., Kotova, E., Andrake, M., Adolf-Bryfogle, J., Glaser, R., Regnard, C., and Tulin, A.V. (2014). Kinase-mediated changes in nucleosome conformation trigger chromatin decondensation via poly(ADP-ribosyl)ation. Mol. Cell 53, 831–842. https://doi.org/10.1016/j.molcel.2014.01.005.

17. Yu, S.W., Andrabi, S.A., Wang, H., Kim, N.S., Poirier, G.G., Dawson, T.M., and Dawson, V.L. (2006). Apoptosis-inducing factor mediates poly(ADP-ribose) (PAR) polymer-induced cell death. Proc. Natl. Acad. Sci. USA 103, 18314–18319. https://doi.org/10.1073/pnas.0606528103.

18. Wang, Y., Kim, N.S., Haince, J.F., Kang, H.C., David, K.K., Andrabi, S.A., Poirier, G.G., Dawson, V.L., and Dawson, T.M. (2011). Poly(ADP-ribose) (PAR) binding to apoptosis-inducing factor is critical for PAR polymerase-1-dependent cell death (parthanatos). Sci. Signal. 4, ra20. https://doi.org/10.1126/scisignal.2000902.

19. Wang, Y., An, R., Umanah, G.K., Park, H., Nambiar, K., Eacker, S.M., Kim, B., Bao, L., Harraz, M.M., Chang, C., et al. (2016). A nuclease that mediates cell death induced by DNA damage and poly(ADP-ribose) polymerase-1. Science 354, aad6872. https://doi.org/10.1126/science.aad6872.

20. Yu, P., Xue, X., Zhang, J., Hu, X., Wu, Y., Jiang, L.H., Jin, H., Luo, J., Zhang, L., Liu, Z., and Yang, W. (2017). Identification of the ADPR binding pocket in the NUDT9 homology domain of TRPM2. J. Gen. Physiol. 149, 219–235. https://doi.org/10.1085/jgp.201611675.

21. Perraud, A.L., Fleig, A., Dunn, C.A., Bagley, L.A., Launay, P., Schmitz, C., Stokes, A.J., Zhu, Q., Bessman, M.J., Penner, R., et al. (2001). ADP-ribose gating of the calcium-permeable LTRPC2 channel revealed by Nudix motif homology. Nature 411, 595–599. https://doi.org/10.1038/35079100.

22. Jacobson, E.L., Cervantes-Laurean, D., and Jacobson, M.K. (1994). Glycation of proteins by ADP-ribose. Mol. Cell. Biochem. 138, 207–212.

23. Xu, Y., Ayrapetov, M.K., Xu, C., Gursoy-Yuzugullu, O., Hu, Y., and Price, B.D. (2012). Histone H2A.Z controls a critical chromatin remodeling step required for DNA double-strand break repair. Mol. Cell 48, 723–733. https://doi.org/10.1016/j.molcel.2012.09.026.

24. Hageman, J., Vos, M.J., van Waarde, M.A.W.H., and Kampinga, H.H. (2007). Comparison of intra-organellar chaperone capacity for dealing with stress-induced protein unfolding. J. Biol. Chem. 282, 34334–34345. https://doi.org/10.1074/jbc.M703876200.

25. Gursoy-Yuzugullu, O., Ayrapetov, M.K., and Price, B.D. (2015). Histone chaperone Anp32e removes H2A.Z from DNA double-strand breaks and promotes nucleosome reorganization and DNA repair. Proc. Natl. Acad. Sci. USA 112, 7507–7512. https://doi.org/10.1073/pnas.1504868112.

26. Alatwi, H.E., and Downs, J.A. (2015). Removal of H2A.Z by INO80 promotes homologous recombination. EMBO Rep. *16*, 986–994. https://doi.org/10.15252/embr.201540330.

27. Xu, Y., Sun, Y., Jiang, X., Ayrapetov, M.K., Moskwa, P., Yang, S., Weinstock, D.M., and Price, B.D. (2010). The p400 ATPase regulates nucleosome stability and chromatin ubiquitination during DNA repair. J. Cell Biol. *191*, 31–43. jcb.201001160.

28. Price, B.D., and D'Andrea, A.D. (2013). Chromatin remodeling at DNA double-strand breaks. Cell *152*, 1344–1354. https://doi.org/10.1016/j.cell.2013.02.011.

29. de Krijger, I., Boersma, V., and Jacobs, J.J.L. (2021). REV7: Jack of many trades. Trends Cell Biol. *31*, 686–701. https://doi.org/10.1016/j.tcb.2021.04.002.

30. Setiaputra, D., and Durocher, D. (2019). Shieldin - the protector of DNA ends. EMBO Rep. *20*, e47560. https://doi.org/10.15252/embr.201847560.

31. Noordermeer, S.M., Adam, S., Setiaputra, D., Barazas, M., Pettitt, S.J., Ling, A.K., Olivieri, M., Álvarez-Quilón, A., Moatti, N., Zimmermann, M., et al. (2018). The shieldin complex mediates 53BP1-dependent DNA repair. Nature *560*, 117–121. https://doi.org/10.1038/s41586-018-0340-7.

32. Mirman, Z., Lottersberger, F., Takai, H., Kibe, T., Gong, Y., Takai, K., Bianchi, A., Zimmermann, M., Durocher, D., and de Lange, T. (2018). 53BP1-RIF1-shieldin counteracts DSB resection through CST- and Polalpha-dependent fill-in. Nature *560*, 112–116. https://doi.org/10.1038/s41586-018-0324-7.

33. Clairmont, C.S., Sarangi, P., Ponnienselvan, K., Galli, L.D., Csete, I., Moreau, L., Adelmant, G., Chowdhury, D., Marto, J.A., and D'Andrea, A.D. (2020). TRIP13 regulates DNA repair pathway choice through REV7 conformational change. Nat. Cell Biol. *22*, 87–96. https://doi.org/10.1038/s41556-019-0442-y.

34. Xie, W., Wang, S., Wang, J., de la Cruz, M.J., Xu, G., Scaltriti, M., and Patel, D.J. (2021). Molecular mechanisms of assembly and TRIP13-mediated remodeling of the human Shieldin complex. Proc. Natl. Acad. Sci. USA *118*, e2024512118. https://doi.org/10.1073/pnas.2024512118.

35. Slade, D., Dunstan, M.S., Barkauskaite, E., Weston, R., Lafite, P., Dixon, N., Ahel, M., Leys, D., and Ahel, I. (2011). The structure and catalytic mechanism of a poly(ADP-ribose) glycohydrolase. Nature *477*, 616–620. https://doi.org/10.1038/nature10404.

36. Barkauskaite, E., Jankevicius, G., Ladurner, A.G., Ahel, I., and Timinszky, G. (2013). The recognition and removal of cellular poly(ADP-ribose) signals. FEBS J. *280*, 3491–3507. https://doi.org/10.1111/febs.12358.

37. Chen, S.H., and Yu, X. (2019). Targeting dePARylation selectively suppresses DNA repair-defective and PARP inhibitor-resistant malignancies. Sci. Adv. *5*, eaav4340. https://doi.org/10.1126/sciadv.aav4340.

38. Kasson, S., Dharmapriya, N., and Kim, I.K. (2021). Selective monitoring of the protein-free ADP-ribose released by ADP-ribosylation reversal enzymes. PLoS One *16*, e0254022. https://doi.org/10.1371/journal.pone.0254022.

39. Ito, R., Sekiguchi, M., Setoyama, D., Nakatsu, Y., Yamagata, Y., and Hayakawa, H. (2011). Cleavage of oxidized guanine nucleotide and ADP sugar by human NUDT5 protein. J. Biochem. *149*, 731–738. https://doi.org/10.1093/jb/mvr028.

40. Pickup, K.E., Pardow, F., Carbonell-Caballero, J., Lioutas, A., Villanueva-Cañas, J.L., Wright, R.H.G., and Beato, M. (2019). Expression of oncogenic drivers in 3D cell culture depends on nuclear ATP synthesis by NUDT5. Cancers *11*, 1337. https://doi.org/10.3390/cancers11091337.

41. Lukas, J., Lukas, C., and Bartek, J. (2011). More than just a focus: the chromatin response to DNA damage and its role in genome integrity maintenance. Nat. Cell Biol. *13*, 1161–1169. https://doi.org/10.1038/ncb2344.

42. Smeenk, G., and van Attikum, H. (2013). The chromatin response to DNA breaks: leaving a mark on genome integrity. Annu. Rev. Biochem. *82*, 55–80. https://doi.org/10.1146/annurev-biochem-061809-174504.

43. Zhou, Y., Liu, L., Tao, S., Yao, Y., Wang, Y., Wei, Q., Shao, A., and Deng, Y. (2021). Parthanatos and its associated components: promising therapeutic targets for cancer. Pharmacol. Res. *163*, 105299. https://doi.org/10.1016/j.phrs.2020.105299.

44. Miller, B.A. (2019). TRPM2 in cancer. Cell Calcium *80*, 8–17. https://doi.org/10.1016/j.ceca.2019.03.002.

45. Wu, X., Wang, L., Ye, Y., Aakre, J.A., Pu, X., Chang, G.C., Yang, P.C., Roth, J.A., Marks, R.S., Lippman, S.M., et al. (2013). Genome-wide association study of genetic predictors of overall survival for non-small cell lung cancer in never smokers. Cancer Res. *73*, 4028–4038. https://doi.org/10.1158/0008-5472.CAN-12-4033.

46. Li, J., Yang, C.C., Tian, X.Y., Li, Y.X., Cui, J., Chen, Z., Deng, Z.L., Chen, F.J., Hayakawa, H., Sekiguchi, M., and Cai, J.P. (2017). MutT-related proteins are novel progression and prognostic markers for colorectal cancer. Oncotarget *8*, 105714–105726. https://doi.org/10.18632/oncotarget.22393.

47. Potter, M., Newport, E., and Morten, K.J. (2016). The Warburg effect: 80 years on. Biochem. Soc. Trans. *44*, 1499–1505. https://doi.org/10.1042/BST20160094.

STAR★METHODS

KEY RESOURCES TABLE

REAGENT or RESOURCE	SOURCE	IDENTIFIER
Antibodies		
NUDT5	Abcam	Cat#ab129172, RRID: AB_11150622
PARG	Abcam	Cat#ab169639
PAR polymer	Trevigen	Cat#4335-MC-100, RRID: AB_2572318
Histone H2A.Z	Cell signaling	Cat#2718, RRID: AB_659840
HA	Abcam	Cat#ab18181, RRID: AB_444303
Acetyl-Histone H4	Millipore	Cat#06-866, RRID: AB_310270
Phospho-Histone H2A.X (Ser139)	Millipore	Cat#05-636, RRID: AB_309864
Phospho-Histone H2A.X (Ser139)	Cell signaling	Cat#2577, RRID: AB_2118010
RPA32/RPA2	Abcam	Cat#ab2175, RRID: AB_302873
RAD51	Cell signaling	Cat#8875, RRID: AB_2721109
53BP1	Abcam	Cat#ab21083, RRID: AB_722496
REV7	Santa Cruz	Cat#sc-135977, RRID: AB_2139534
Phospho-KAP1 (S824)	Bethyl	Cat#A300-767A, RRID: AB_669740
KAP1	Bethyl	Cat#A300-274A, RRID: AB_185559
FLAG	Sigma	Cat#F1804, RRID: AB_262044
β-actin	Santa Cruz	Cat#sc-47778, RRID: AB_626632
Chemicals, peptides, and recombinant proteins		
NUDT5 inhibitor TH5427	Dr Thomas Helleday's lab	N/A
PARP inhibitor Olaparib	Selleck	Cat#S1060, CAS 763113-22-0
PARG inhibitor DEA	Trevigen	Cat#4680-096-03
Bleomycin	Novaplus	Cat#NDC 0409-0332-20
Hydrogen peroxide	Sigma-Aldrich	Cat#H1009, CAS 7722-84-1
Camptothecin	Sigma-Aldrich	Cat#C9911, CAS 7689-03-4
2-Deoxy-D-glucose	Sigma-Aldrich	Cat#D8375, CAS 154-17-6
Sodium Azide	Sigma-Aldrich	Cat#S8032, CAS 26628-22-8
Oligomycin A	Sigma-Aldrich	Cat#75351, CAS 579-13-5
D-Luciferin	GoldBio	Cat#LUCK-100, CAS 115144-35-9
Critical commercial assays		
CellTiter-Glo® Luminescent Cell Viability Assay	Promega	Cat#G7571
SimpleChIP® Plus Sonication Chromatin IP Kit	Cell signaling	Cat#56383
FITC BrdU Flow Kit	BD Pharmingen™	Cat#559619, RRID: AB_2617060
Deposited data		
Raw RNA-seq data	This paper	GEO accession number: GSE196718
Experimental models: Cell lines		
Human: U-2 OS	ATCC	HTB-96
Human: HEK293T	ATCC	CRL-3216
Human: T-47D	ATCC	HTB-133
Human: U-2 OS DR-GFP	Dr Jeremy Stark's lab	N/A
Human: HeLa-NHEJ	Dr Jeremy Stark's lab	N/A
Human: HeLa-altEJ	Dr Jeremy Stark's lab	N/A
Human: U-2 OS TRIP13−/−	Dr Alan D'Andrea's lab	N/A
Oligonucleotides		
siNUDT5#1	IDT	hs.Ri.NUDT5.13.1
siNUDT5#2	IDT	hs.Ri.NUDT5.13.2

Continued

REAGENT or RESOURCE	SOURCE	IDENTIFIER
siNUDT5#3	IDT	hs.Ri.NUDT5.13.3
siPARG#1	IDT	hs.Ri.PARG.13.1
siPARG#2	IDT	hs.Ri.PARG.13.2
siH2A.Z	IDT	hs.Ri.H2AFZ.13.1
Primers for P84-ZFN, See Table S1	This paper	N/A
Recombinant DNA		
pCMV6-ENTRY-NUDT5-MycDDK	Origene	N/A
Luciferase-Nuclear	Dr Miguel Beato's lab	N/A
P84-ZFN	Dr Michael C. Holmes's lab	N/A
BFP-I-SceI	Dr Daphne Haas-Kogan's lab	N/A
Software and algorithms		
GraphPad Prism		URL: http://www.graphpad.com/
CytoExpert		URL: https://www.beckman.com/flow-cytometry/instruments/cytoflex/software
ImageJ		URL: https://imagej.nih.gov/ij/

RESOURCE AVAILABILITY

Lead contact
Further information and requests for resources and reagents should be directed to and will be fulfilled by the lead contact, Brendan D. Price (brendan_price@dfci.harvard.edu).

Materials availability
This study did not generate new unique reagents.

Data and code availability
- Transcriptomics and RNAseq data have been deposited with Gene Expression Omnibus (GEO) and are publicly available as of the date of publication. Accession numbers are listed in the key resources table.
- This paper does not report original code.
- Any additional information required to reanalyze the data reported in this paper is available from the lead contact upon request.

EXPERIMENTAL MODEL AND SUBJECT DETAILS

Cell lines and reagents
U2OS, HEK293T and HeLa cells were cultured in Dulbecco's modified Eagle's medium (Gibco, Thermo Fisher, Cat#11995073) containing 10% fetal bovine serum(Gibco, Thermo Fisher, Cat#10437028).

METHODS DETAILS

Cell lines and transfection
Plasmids were transfected using Lipofectamine 2000 (Thermo Fisher Scientific). Small interfering RNAs were transfected using Lipofectamine RNAiMAX (Thermo Fisher Scientific).

DSB repair reporter assays
U2OS cells expressing the DR-GFP reporter, HeLa cells expressing the EJ5 reporter or HeLa cells expressing the EJ2 reporter were transfected with BFP-I-SceI plasmid using Lipofectamine 2000 (Invitrogen, CA). 48hr later cells were trypsinized and analyzed on the Cytoflex (Beckman, CA). BFP signal was used to identify I-SceI expressing cells. Percentage of GFP positive cells were analyzed using CytoExpert software (Beckman, CA). For Figure 1A, reporter cells were transfected with each siRNA 24hr before I-SceI transfection. For Figure 1B, each cell line was treated with 10 μM TH5427 for 4 h before I-SceI transfection. For Figure 4E, DR-GFP reporter cells were treated with 2-Deoxy-D-glucose at the indicated concentration for 6 h before I-SceI transfection. For Figure 4E, DR-GFP reporter cells were transfected with siH2A.Z on day 1, siNUDT5 on day 2, and I-SceI was transfected on day 3.

Clonogenic cell survival assay

U2OS cells were plated in triplicate on 6-well dishes and allowed to attach for 24 hr. Cells were treated with 10 μM TH5427 for 4 h before radiation. After 12 days of recovery cells were fixed and stained with 10% ethanol containing 2.5% (w/v) crystal violet. Colonies with >50 cells were counted.

ATP measurement

For total cellular ATP measurement, we used CellTiter-Glo Luminescent Cell Viability Assay (Promega). U2OS cells were plated in white opaque 96 well plates. Prior to measurement, 100 μL of CellTiter-Glo reagent was added into each well and the contents were mixed for 2 min on an orbital shaker to induce cell lysis. The relative amounts of ATP were then measured using the biolumi-nescence plate reader (CLARIOstar PLUS, BMG Inc, NC, USA). For Figure 4B, siRNAs were transfected 48hrs before measurement. For Figures 4A, 4D, and S4D, cells were preincubated in DMSO (solvent, 4hr), TH5427(10 μM, 4hr), Olaparib (5 μM, 1hr), DEA (1 μM, 1hr) or in combination and H_2O_2 (100 μM) was added at the indicated time before measurement.

For nuclear ATP measurement, U2OS cells were transfected with the GFP-NucLuc construct. Cells were plated in white opaque 96 well plates and cultured overnight before measurement. Prior to measurement the culture medium was replaced with PBS containing 150 μg/mL D-luciferin and incubated for 10 min. The relative amounts of ATP were then measured using the bioluminescence plate reader. For Figure 4C, cells were preincubated in DMSO (solvent) or TH5427(10 μM) for 4 h and H_2O_2 (100 μM) was added at the indicated time before measurement. For Figure S3E, the ATP depleting agents were added 30 min before measurement. For Figure S3G, 2-Deoxy-D-glucose was added at the indicated concentration 24hrs before measurement.

Laser microirradiation

U2OS cells were seeded onto #1.5 cover glasses. Micro-irradiation was performed on a Zeiss PALM MicroBeam system equipped with a 355 nm UV laser source ($E < 60$ uJ, $f = 1000$ Hz, $t < 2$ ns). The laser micro-irradiation was focused and delivered through a 63× object (LD Plan-Neofluar 63×/0.75Corr) of a Zeiss Observer Z1 microscope. The power of output (cut) was set at 34% and the speed of cutting was set at 50%. After recovery at 37°C incubator for the indicated time, cells were fixed with 4% PFA for 10 min. Cells were then permeabilized with PBS supplemented with 0.2% Triton X-100 for 5 min and blocked with PBS containing 1% BSA and 0.3% Triton X-100 for 30 min. Cells were then incubated with primary antibody diluted in blocking buffer at 4°C overnight. The cells were washed with PBS three times and incubated with fluorophore-conjugated secondary antibodies plus Hoechst 33,342 for 1 h. The cells were washed with PBS three times and mounted in Fluoromount-G (Electron Microscopy Sciences) before imaging. siRNAs were transfected 48hrs before laser microirradiation. siRNAs were transfected 48 h before laser microirradiation. Olaparib (5 μM) and DEA (1 μM) were added 1 h before laser microirradiation. TH5427 (10 μM) was added 4 h before laser microirradiation.

DSB generation and ChIP assays

293T cells were transfected with either P84-ZFN or pcDNA3.1 and allowed to recover for 18 h in the incubator. Cells were fixed in 1% methanol-free formaldehyde for 10 min to crosslink proteins, then lysed in ChIP buffer (Cell Signaling Technology, MA, USA), son-icated (Sonic 250, Fisher Scientific), and cleared by centrifugation. All ChIP was performed using the SimpleChIP Plus Sonication Chromatin IP Kit with magnetic beads according to the manufacturer's instructions (Cell Signaling Technologies, MA). DNA levels were quantified by qPCR amplification using Power SYBR Green Mastermix (Applied Biosystems, MA) and primer sets proximal to the P84-ZFN cut site at the PPP1R12C gene locus. For Figure 2C, 293T cells were transfected with Flag-NUDT5 24 h before P84-ZFN transfection. For Figure 4E, 293T cells were transfected with HA-H2A.Z 24 h before P84-ZFN transfection.

Co-immunoprecipitation

U2OS cells expressing Flag-NUDT5 were treated with H_2O_2 (100 μM) or vehicle (control). Cell extracts were harvested and processed for co-immunoprecipitation using anti-FLAG antibody or IgG (control). 10% of each input and immunoprecipitated proteins were separated by SDS-page gel electrophoresis and the presence of PARG and NUDT5 detected using anti-PARG antibody (abcam ab169639) and anti-NUDT5 (ab129172).

RNA-seq

U2OS cells were transfected with siCtrl or siNUDT5. 48 h later total RNA was extracted using RNeasy Mini kit (Qiagen) and polya-denylated (polyA+) transcripts were enriched using oligo-dT coated beads. The polyA + RNA is subsequently fragmented using heat and Mg+ and reverse transcribed into cDNA using random priming. Illiumina adapters are ligated to dsDNA and PCR amplified. Libraries were prepared using Roche Kapa mRNA HyperPrep strand specific sample preparation kits from 200ng of purified total RNA according to the manufacturer's protocol on a Beckman Coulter Biomek i7. The finished dsDNA libraries were quantified by Qubit fluorometer and Agilent Tape Station 4200. Uniquely dual indexed libraries were pooled in an equimolar ratio and shallowly sequenced on an Illumina MiSeq to further evaluate library quality and pool balance. The final pool was sequenced on an Illumina NovaSeq 6000 with paired-end 100bp reads at the Dana-Farber Cancer Institute Molecular Biology Core Facilities. Sequenced reads were aligned to the UCSC hg19 reference genome assembly and gene counts were quantified using STAR (v2.7.3a). Differential gene expression testing was performed by DESeq2 (v1.22.1). RNA-seq analysis was performed using the VIPER snakemake pipeline.

Irradiation-induced foci assay

U2OS cells were seeded onto #1.5 cover glasses and transfected with siRNAs. 48 h later cells were treated with radiation and allowed to recover for the indicated time in the incubator. Cells were fixed first with 1% PFA/0.5% Triton X-100 in PBS for 20 min, then with 1% PFA/0.3% Triton X-100 in PBS containing 0.5% methanol for 20 min. Cells were blocked with PBS containing 1mg/ml BSA, 0.5% Triton X-100, 3% goat serum, 1mM EDTA for 1 h. Cells were then incubated with primary antibody diluted in blocking buffer at 4°C overnight. The cells were washed with PBS three times and incubated with fluorophore-conjugated secondary antibodies plus Hoechst 33,342 for 1 h. The cells were washed with PBS three times and mounted in Fluoromount-G (Electron Microscopy Sciences) before imaging.

Cell cycle analysis

Cell cycle analysis were processed using the FITC BrdU Flow Kit (BD Biosciences, USA) according to the manufacturer's instructions. Briefly, U2OS cells were incubated with 10 μM BrdU for 30 min before fixed with BD Cytofix/Cytoperm Buffer and Permeabilized with BD Cytoperm Permeabilization Buffer Plus. Then the cells were treated with DNase to expose BrdU epitopes and immunofluorescent stained with fluorochrome-conjugated anti-BrdU. DNA was stained using 7-AAD before analyzing on Cytoflex (Beckman). For Figure S1B, U2OS cells were transfected with siNUDT5 48 h before cell cycle analysis. For Figures S3H and S3I, U2OS cells were treated with 2-Deoxy-D-glucose for 24 h before cell cycle analysis.

QUANTIFICATION AND STATISTICAL ANALYSIS

Western blot images were quantitated using ImageJ, and foci formation images quantitated using ImageJ software packages. RNA-seq data was analyzed using the VIPER snakemake pipeline. Statistical analysis were performed in GraphPad Prism version 9 (San Diego, CA). Error bars indicate the standard error of the mean. It was assumed that all data were normally distributed. Data were analyzed using unpaired two-tailed Student's t-tests. p values of <0.05 were considered statistically significant (*$p < 0.05$, **$p < 0.01$, ***$p < 0.001$ and ****$p < 0.0001$).